EARTHQUAKE ENGINEERING AND STRUCTURAL DYNAMICS
Earthquake Engng Struct. Dyn. 2009; **00**:1–16 *Prepared using* eqeauth.cls *[Version: 2002/11/11 v1.00]*

Incremental Dynamic Analysis for Estimating Seismic Performance Sensitivity and Uncertainty‡

Dimitrios Vamvatsikos[1,*,†] and Michalis Fragiadakis[2]

[1] *Department of Civil and Environmental Engineering, University of Cyprus, Nicosia 1678, Cyprus*
[2] *School of Civil Engineering, National Technical University of Athens, Greece*

SUMMARY

Incremental Dynamic Analysis (IDA) is presented as a powerful tool to evaluate the variability in the seismic demand and capacity of non-deterministic structural models, building upon existing methodologies of Monte Carlo simulation and approximate moment-estimation. A nine-story steel moment-resisting frame is used as a testbed, employing parameterized moment-rotation relationships with non-deterministic quadrilinear backbones for the beam plastic-hinges. The uncertain properties of the backbones include the yield moment, the post-yield hardening ratio, the end-of-hardening rotation, the slope of the descending branch, the residual moment capacity and the ultimate rotation reached. IDA is employed to accurately assess the seismic performance of the model for any combination of the parameters by performing multiple nonlinear timehistory analyses for a suite of ground motion records. Sensitivity analyses on both the IDA and the static pushover level reveal the yield moment and the two rotational-ductility parameters to be the most influential for the frame behavior. To propagate the parametric uncertainty to the actual seismic performance we employ a) Monte Carlo simulation with latin hypercube sampling, b) point-estimate and c) first-order second-moment techniques, thus offering competing methods that represent different compromises between speed and accuracy. The final results provide firm ground for challenging current assumptions in seismic guidelines on using a median-parameter model to estimate the median seismic performance and employing the well-known square-root-sum-of-squares rule to combine aleatory randomness and epistemic uncertainty. Copyright © 2009 John Wiley & Sons, Ltd.

KEY WORDS: performance-based earthquake engineering; incremental dynamic analysis; epistemic uncertainty; monte carlo; latin hypercube sampling; first-order second-moment

1. INTRODUCTION

The accurate estimation of the seismic demand and capacity of structures stands at the core of performance-based earthquake engineering. Still, seismic performance is heavily influenced by both aleatory randomness, e.g., due to natural ground motion record variability, and epistemic

*Correspondence to: Dimitrios Vamvatsikos, 75 Kallipoleos Str, PO Box 20537, Nicosia 1678, Cyprus.
†E-mail: divamva@ucy.ac.cy
‡Based on short papers presented at the 1st European Conference on Earthquake Engineering and Seismology, Geneva, 2006 and at the 14th World Conference on Earthquake Engineering, Beijing, 2008.

Received ? September 2008
Revised ? February 2008
Accepted ? February 2009

uncertainty, owing to modeling assumptions, omissions or errors. Ignoring their effect means that structures are being designed and built without solid data or even adequate understanding of the expected range of behavior. While guidelines have emerged (e.g., SAC/FEMA [1]) that recognize the need for assessing epistemic uncertainties by explicitly including them in estimating seismic performance, this role is usually left to ad hoc safety factors, or, at best, standardized dispersion values that often serve as placeholders. So, if one wanted to actually compute the variability in the seismic behavior due to parameter uncertainty, the question still remains: What would be a good way to do so?

As a partial answer to this issue, there have been several attempts to isolate some useful cases and gain insight into the effect of the properties of a model to its estimated seismic performance. For example, Luco and Cornell [2, 3] found that random connection fractures have a detrimental effect on the dynamic response of steel moment-resisting frames while Foutch and Shi [4] used different hysteretic models to show the effect of hysteresis of moment connections on global demand. Perhaps the most exhaustive study on the influence of model parameters on global collapse capacity has been performed by Ibarra [5] who studied the dynamic instability of oscillators and idealized single-bay frames with beam-column connections having non-trivial backbones including both cyclic and in-cycle degradation. Finally, Porter *et al.* [6], have discussed the sensitivity of loss estimation to structural modeling parameters in order to discern the most influential variables.

Such studies have offered a useful look into the sensitivity of structures to uncertain parameters. Yet, only Ibarra [5] actually proposes a method to propagate the uncertainty from model parameters to structural behavior using first-order-second-moment (FOSM) principles verified through Monte Carlo to evaluate the collapse capacity uncertainty. Lee and Mosalam [7] have also used FOSM to determine the response uncertainty of a reinforced-concrete (RC) shear wall structure to several modeling parameters. However, in our opinion, two of the most important contributions in this field have come from parallel research efforts that proposed the use of Monte Carlo simulation [8] within the framework of IDA (Vamvatsikos and Cornell [9]) to incorporate parameter uncertainty. Liel *et al.* [10] used IDA with Monte Carlo and FOSM coupled with a response surface approximation method to evaluate the collapse uncertainty of an RC building. On a similar track, Dolsek [11] has proposed using Monte Carlo with efficient Latin Hypercube Sampling (LHS) on IDA to achieve the same goal. While both methods were only applied on RC frame structures and only discussed the estimation of uncertainty for collapse or near-collapse limit-states, they are fairly generalizable and applicable to a variety of building types and limit-states.

Working independently of the above research teams, we have also come to similar conclusions on the use of Monte Carlo and simpler moment-estimation techniques to estimate seismic performance uncertainty. Thus, in light of existing research, we aim to present our own view on the use of IDA to offer a comprehensive solution to the issue of model-parameter uncertainty, while drawing useful conclusions on the effects of uncertainties along the way. IDA being a resource-intensive method, we will attempt to economically tap into its power through computation-saving methods. Efficient Monte Carlo simulation and moment-estimation techniques will also be employed to propagate the uncertainty from parameters to the IDA-evaluated seismic performance offering different compromises in speed and accuracy. Using a well-studied steel moment-resisting frame as a testbed and focusing on the plastic-hinge modeling uncertainties, we will nevertheless present a general methodology that is applicable to a wide range of structures.

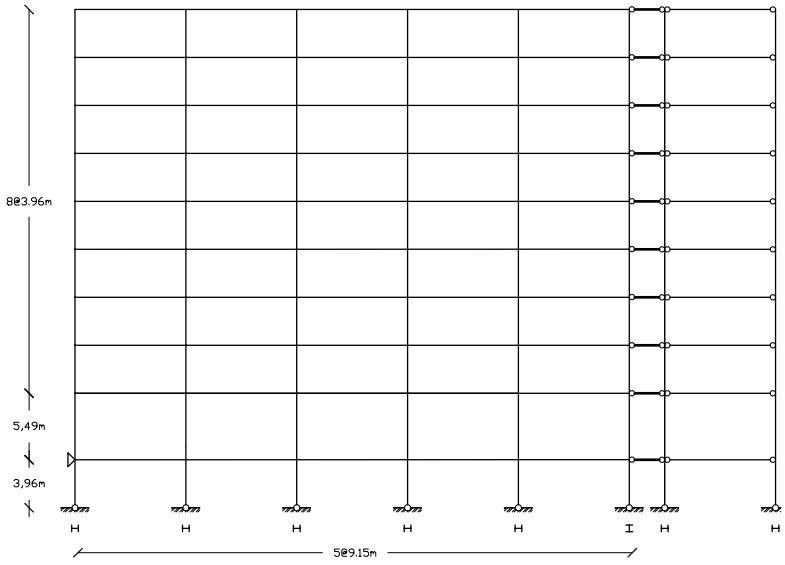

Figure 1. The LA9 steel moment-resisting frame.

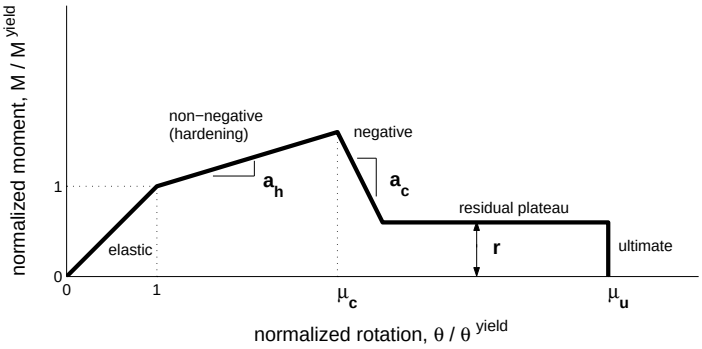

Figure 2. The moment-rotation beam-hinge backbone to be investigated and its six controlling parameters.

2. MODEL DESCRIPTION

The structure selected is a nine-story steel moment-resisting frame with a single-story basement (Figure 1) that has been designed for Los Angeles, following the 1997 NEHRP (National Earthquake Hazard Reduction Program) provisions (Foutch and Yun [12]). A centerline model with nonlinear beam-column connections was formed using OpenSees (McKenna *et al.* [13]). It allows for plastic hinge formation at the beam ends while the columns are assumed to remain elastic. This has been a conscious choice on our part: Despite the rules of capacity design,

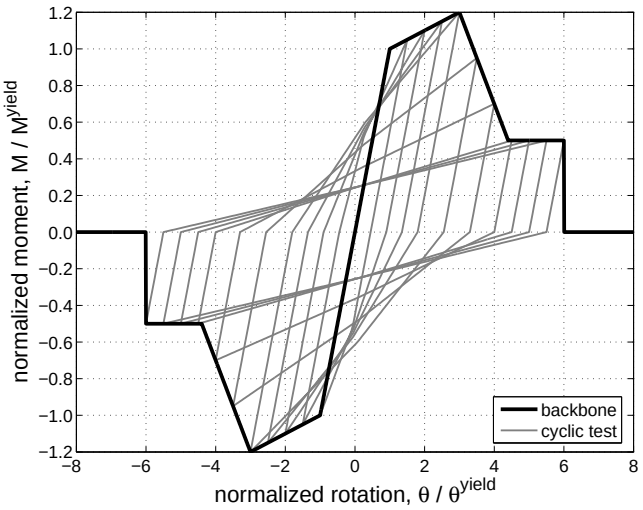

Figure 3. The backbone and hysteretic loops of the base-case hinge.

there is always the possibility of a column yielding earlier than the connecting beams, an issue aggravated by uncertain yield strengths. Preliminary tests found this effect to be minor for this nine-story structure, especially when high correlation was assumed between the steel strengths of beams and columns.

The structural model also includes P-Δ effects while the internal gravity frames have been directly incorporated (Figure 1). The fundamental period of the reference frame is $T_1 = 2.35$s and accounts for approximately 84% of the total mass. Essentially this is a first-mode dominated structure that still allows for significant sensitivity to higher modes. Previous studies (e.g., Fragiadakis *et al.* [14]) have identified the yield strength of the hinges as the most influential parameter in a steel frame, compared to story mass and stiffness, for displacement-related quantities. While stiffness might prove to be a more important parameter for floor accelerations and contents' damage, we will only focus on drift-sensitive structural and non-structural damage. Thus, studying the influence of the beam-hinge properties on the structural performance of the building will be our goal.

The beam-hinges are modeled as rotational springs with a quadrilinear moment-rotation backbone (Figure 2) that is symmetric for positive and negative rotations (Ibarra [5]). The backbone hardens after a yield moment of a_{My} times the nominal, having a non-negative slope of a_h up to a normalized rotation (or rotational ductility) μ_c where the negative stiffness segment starts. The drop, at a slope of a_c, is arrested by the residual plateau appearing at normalized height r that abruptly ends at the ultimate rotational ductility μ_u. The spring employs a moderately pinching hysteresis without any cyclic degradation, as shown in Figure 3.

This complex model is versatile enough to simulate the behavior of numerous moment-connections, from ductile down to outright fracturing. A "base" hinge was defined using the properties $a_{\mathrm{My}} = 1$, $a_h = 10\%$, $\mu_c = 3$, $a_c = -50\%$, $r = 50\%$ and $\mu_u = 6$, which were assumed to be the mean-values for all beam-column connections. Thus we have formed a reference frame that will serve as the basis for comparing all our modified models.

Table I. The suite of thirty ground motion records used.

No	Event	Station	ϕ° *	Soil†	M‡	R§(km)	PGA(g)
1	Loma Prieta, 1989	Agnews State Hospital	090	C,D	6.9	28.2	0.159
2	Northridge, 1994	LA, Baldwin Hills	090	B,B	6.7	31.3	0.239
3	Imperial Valley, 1979	Compuertas	285	C,D	6.5	32.6	0.147
4	Imperial Valley, 1979	Plaster City	135	C,D	6.5	31.7	0.057
5	Loma Prieta, 1989	Hollister Diff. Array	255	–,D	6.9	25.8	0.279
6	San Fernando, 1971	LA, Hollywood Stor. Lot	180	C,D	6.6	21.2	0.174
7	Loma Prieta, 1989	Anderson Dam Downstrm	270	B,D	6.9	21.4	0.244
8	Loma Prieta, 1989	Coyote Lake Dam Downstrm	285	B,D	6.9	22.3	0.179
9	Imperial Valley, 1979	El Centro Array #12	140	C,D	6.5	18.2	0.143
10	Imperial Valley, 1979	Cucapah	085	C,D	6.5	23.6	0.309
11	Northridge, 1994	LA, Hollywood Storage FF	360	C,D	6.7	25.5	0.358
12	Loma Prieta, 1989	Sunnyvale Colton Ave	270	C,D	6.9	28.8	0.207
13	Loma Prieta, 1989	Anderson Dam Downstrm	360	B,D	6.9	21.4	0.24
14	Imperial Valley, 1979	Chihuahua	012	C,D	6.5	28.7	0.27
15	Imperial Valley, 1979	El Centro Array #13	140	C,D	6.5	21.9	0.117
16	Imperial Valley, 1979	Westmoreland Fire Station	090	C,D	6.5	15.1	0.074
17	Loma Prieta, 1989	Hollister South & Pine	000	–,D	6.9	28.8	0.371
18	Loma Prieta, 1989	Sunnyvale Colton Ave	360	C,D	6.9	28.8	0.209
19	Superstition Hills, 1987	Wildlife Liquefaction Array	090	C,D	6.7	24.4	0.18
20	Imperial Valley, 1979	Chihuahua	282	C,D	6.5	28.7	0.254
21	Imperial Valley, 1979	El Centro Array #13	230	C,D	6.5	21.9	0.139
22	Imperial Valley, 1979	Westmoreland Fire Station	180	C,D	6.5	15.1	0.11
23	Loma Prieta, 1989	Halls Valley	090	C,C	6.9	31.6	0.103
24	Loma Prieta, 1989	WAHO	000	-,D	6.9	16.9	0.37
25	Superstition Hills, 1987	Wildlife Liquefaction Array	360	C,D	6.7	24.4	0.2
26	Imperial Valley, 1979	Compuertas	015	C,D	6.5	32.6	0.186
27	Imperial Valley, 1979	Plaster City	045	C,D	6.5	31.7	0.042
28	Loma Prieta, 1989	Hollister Diff. Array	165	–,D	6.9	25.8	0.269
29	San Fernando, 1971	LA, Hollywood Stor. Lot	090	C,D	6.6	21.2	0.21
30	Loma Prieta, 1989	WAHO	090	–,D	6.9	16.9	0.638

* Component † USGS, Geomatrix soil class ‡ moment magnitude §closest distance to fault rupture

3. PERFORMANCE EVALUATION

Incremental Dynamic Analysis (IDA, Vamvatsikos and Cornell [9]) is a powerful analysis method that can provide accurate estimates of the complete range of the model's response, from elastic to yielding, then to nonlinear inelastic and finally to global dynamic instability. To perform IDA we will use a suite of thirty *ordinary* ground motion records (Table I) representing a scenario earthquake. These belong to a bin of relatively large magnitudes of 6.5–6.9 and moderate distances, all recorded on firm soil and bearing no marks of directivity. IDA involves performing a series of nonlinear dynamic analyses for each record by scaling it to multiple levels of intensity. Each dynamic analysis is characterized by two scalars, an Intensity Measure (IM), which represents the scaling factor of the record, and an Engineering Demand Parameter (EDP) (according to current Pacific Earthquake Engineering Research Center terminology), which monitors the structural response of the model.

For moderate-period structures with no near-fault activity, an appropriate choice for the IM is the 5%-damped first-mode spectral acceleration $S_a(T_1, 5\%)$. While this selection is made easier by the fact that we chose to vary strengths only, thus maintaining a constant first-mode period, it can nevertheless prove useful beyond this limited example. Even under stiffness and

mass uncertainties, the fundamental period of the base-case frame, T_1^{base}, can still serve as a reliable reference point, as shown, for example, by the results of Vamvatsikos and Cornell [15]. Therefore, $S_a(T_1^{\text{base}}, 5\%)$ can be recommended for general use, avoiding simpler but less efficient IMs, such as the peak ground acceleration [9]. Regarding the building's response, as we have previously discussed, our focus is on deformation-sensitive structural and non-structural damage. Therefore, the maximum interstory drift, $\theta_{\max}$, of the structure is a good candidate for the EDP.

It should be noted that recent studies have shown that simply using $S_a(T_1, 5\%)$ as the IM will generate biased results when using large scale factors (Luco and Bazzurro [16]). Unfortunately, the limitations of the existing record catalogue do not allow us to refrain from scaling, which was the basis of IDA after all. As observed by Luco and Bazzurro [16], these differences are mainly an effect of spectral shape, something that can be corrected e.g., by considering improved scalar or vector IMs that include spectral shape parameters, as proposed at by Vamvatsikos and Cornell [15], Luco and Cornell [17] and Baker and Cornell [18]. Nevertheless, we will maintain the use of $S_a(T_1, 5\%)$ for the benefit of the readers, since it makes for better understanding of the IDA curves. Renormalizing to another IM is actually trivial and only a matter of postprocessing [15]. Furthermore, sufficiency and bias are actually most important when combining IDA results with hazard information. Since we will not be engaging in any such calculations, we are safe to proceed with running the analysis with $S_a(T_1, 5\%)$.

Using the *hunt&fill* algorithm (Vamvatsikos and Cornell [19]) allows capturing each IDA curve with only twelve runs per record. Appropriate interpolation techniques allow the generation of a continuous IDA curve in the IM-EDP plane from the discrete points obtained by the dynamic analyses. Such results are in turn summarized to produce the median and the 16%, 84% IDA curves that can accurately characterize the distribution of the seismic demand and capacity of the structure for frequent or rarer ground motion intensities.

Having such a powerful, albeit resource-intensive, tool at our disposal, we are left with the selection of the alternate models to evaluate. There is obviously an inexhaustible number of variations one could try with the six parameters of the adopted plastic hinge, not including the possibility of having different hinge models in each story, or even for each individual connection. In the course of this study we chose to vary all six backbone parameters, namely a_h, μ_c, a_c, r, μ_u and a_{My}, independently from each other but uniformly throughout the structure. Thus, a perfect, positive *spatial* correlation of the beam hinges has been adopted: All beam-column connections in the model have the same *normalized* properties, a deliberate choice that is expected to substantially increase the parameters' influence on the results.

Contrary to our assessment above, it could be argued that non-perfect correlation of the hinges in the structure might cause strength irregularities that can lead to a higher variability in the response. Still, for strong-column, weak-beam moment-frames with rigid diaphragms it is the combined response of all hinges within a story that defines its response, not the individual strength. Therefore, such irregularities will not arise unless there is high positive correlation within the hinges of each story but no, or negative, correlation from story to story, an unrealistic assumption in general. Weak-column, strong-beam designs can further magnify such effects. Since the above conditions do not apply in our nine-story structure, it makes sense to expect relatively high variabilities as an outcome of our assumptions.

In the following sections, we evaluate the effect of the six parameters, first by varying them individually, one at a time, to perform sensitivity analysis and then concurrently for uncertainty analysis.

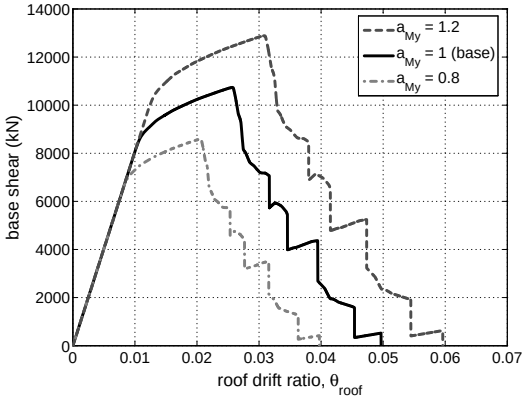

(a) a_{My} influences global strength and θ_{roof} capacity

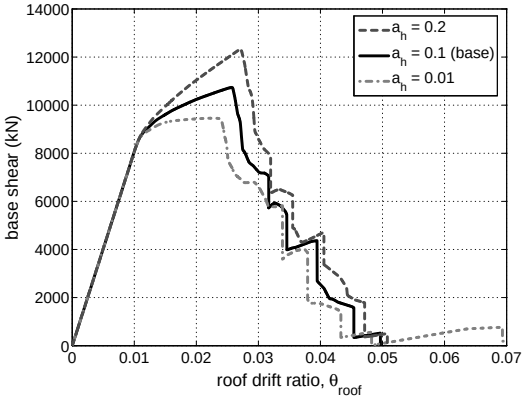

(b) a_h modifies global strength

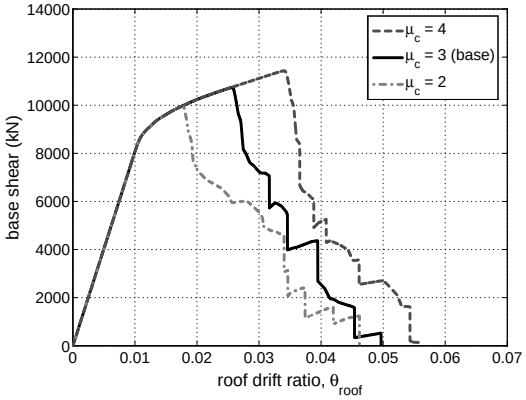

(c) Increased μ_c leads to higher ductilities

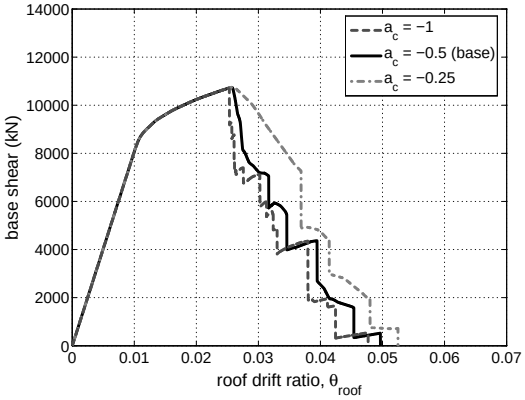

(d) a_c is moderately influential

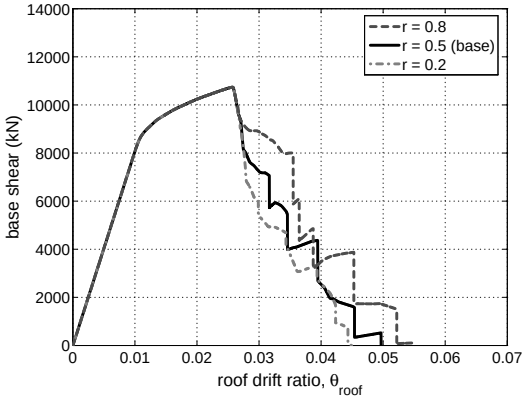

(e) r is of minor importance

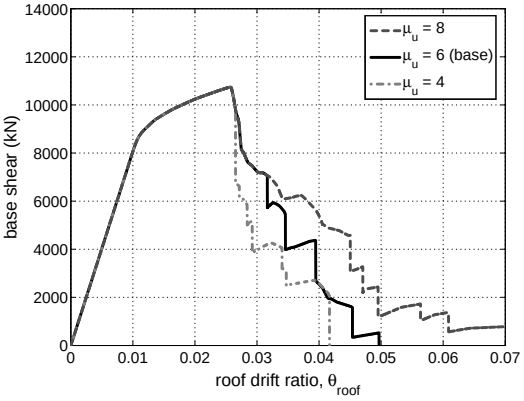

(f) Decreasing μ_u reduces the system ductility

Figure 4. Sensitivity of the SPO curves to the beam-hinge backbone parameters.

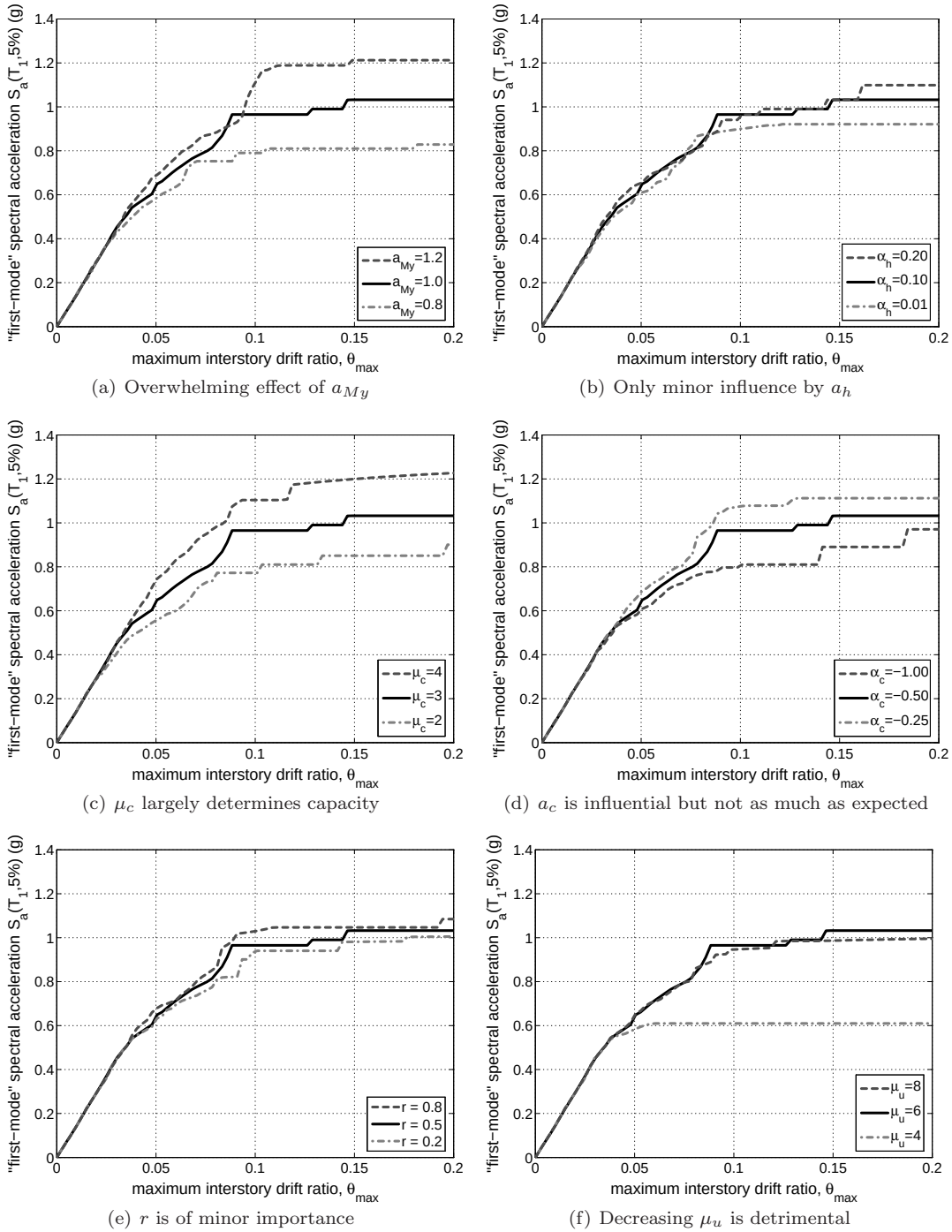

(a) Overwhelming effect of a_{My}

(b) Only minor influence by a_h

(c) μ_c largely determines capacity

(d) a_c is influential but not as much as expected

(e) r is of minor importance

(f) Decreasing μ_u is detrimental

Figure 5. Sensitivity of the median IDA curves to the beam-hinge backbone parameters.

4. SENSITIVITY ANALYSIS

To evaluate the behavior of our model we performed a sensitivity study by perturbing each of the six backbone parameters independently of each other and only one at a time, pushing each random parameter above and below its central, base-case, value. The sensitivity of each parameter is evaluated using both static pushover and IDA for the following pairs of modifications: $a_{\mathrm{My}} = \{0.8, 1.2\}$, $a_h = \{1\%, 20\%\}$, $\mu_c = \{2, 4\}$, $a_c = \{-100\%, -25\%\}$, $r = \{20\%, 80\%\}$ and $\mu_u = \{4, 8\}$.

4.1. Static pushover sensitivity

While IDA is indeed a powerful tool, making sense of its complexity is often difficult without performing a static pushover (SPO) analysis first. Despite criticism on its performance-estimation abilities, the pushover is a simple method that offers useful intuition on the expected behavior of a structural model. It has been shown to correspond to the fractile IDA curves [9], thus helping us understand and qualitatively predict the dynamic behavior of the structure. Therefore, static pushover analysis with a first-mode lateral load pattern has been performed as a preliminary evaluation of the performance sensitivity of the base-case versus the modified curves shown in Figures 4(a–f). Therein, plotted in base shear versus roof drift ratio θ_{roof} coordinates, the response of the base-case frame always appears as a solid line in the middle, while the upgraded and degraded parameter curves fan around its sides.

The effect of a_{My} appears in Figure 4(a) and it is indeed impressive. As expected, the connection yield moment is directly related to the global strength and deformation capacity of the system; increasing a_{My} by 20% provides a beneficial effect practically everywhere on the SPO curve, improving the maximum base shear by 22% and increasing the maximum attainable roof drift by a similar amount. Figure 4(b) shows the effect of the post-yield hardening slope a_h. Clearly, increasing the slope to 10% seems to raise the SPO curve to the second highest base shear observed in any of the cases studied, while it slightly delays its drop due to fracturing. Lowering a_h to almost zero has the exact opposite effect. Still, when the negative slope takes over and the SPO starts dropping, it becomes hard to find any considerable differences. Connections in stories different from the one where fracturing has occurred may indeed be enjoying the benefits of a higher (or lower) hardening, but the sheer loss of strength seems to nullify this effect anywhere beyond 3% roof drift.

On the other hand, increasing the μ_c in Figure 4(c) to a value of 4 instead of 3 seems to have a much more substantial effect. The fracturing drop is delayed at least by a 0.8% roof drift, while there is a moderate increase in the maximum load. Similarly, lowering μ_c to only 2 has the inverse effect, forcing the SPO to lose strength earlier, both in force and deformation terms. Even when fracturing occurs, the changes in μ_c still seem to help, even if only by a little: The three curves follow converging descents that end in relatively close values of roof drift. Unsurprisingly, both a_h and μ_c expend most of their influence in the pre-fracturing nonlinear range, as they both control the hardening, positive stiffness segment but have little, if any, control on the segments that follow. Figure 4(b) shows a rather minor influence of the negative slope a_h on the system performance. Reducing the descent slope to 25% seems to help the post-fracture performance, but only marginally. Making it steeper seems to have an even smaller effect. The reason is obviously the relatively high base-case value of $r = 0.5$ which means that no matter how fast the connection loses strength, it will maintain a healthy 50%

residual strength that will always boost its performance. Had we used a lower central r-value the results would probably have been quite different.

The final two parameters, namely r and μ_u, only influence the hinge behavior beyond the negative drop. Therefore in Figures 4(e) and 4(f) we see no change at all in the SPO curves before the loss of strength occurs. Afterwards, it is obvious that increasing the height of the residual plateau r is less useful than increasing its length μ_u before the ultimate failure. The former only provides some marginal benefits in the post-fracture area, while the latter is the best way to extend the SPO curve of the building to roof drifts higher than 7%, while maintaining somewhat higher strengths than the base case. Similarly, reducing r to 20% makes only a small difference while decreasing μ_u seems to force an earlier collapse of the structure: The drop to zero strength now appears at about 4% versus the 5% of the base case.

4.2. IDA sensitivity

Having studied the SPO curves, we have now formed an idea on what to expect qualitatively from dynamic analysis. Still, there is only so much that we can discern using just static results. Therefore, for each modified frame we performed IDA to evaluate the sensitivity of the seismic performance which we chose to express by comparing, in IM-terms, the median IDA curves of the base case versus the modified ones appearing in Figures 5(a-f). Keeping in mind that only thirty records were used to trace the median IDA curves shown, we should discount small differences as statistically insignificant. Thus we can safely state that a modified structure is better or worse-performing than the base case only when its median IDA appears at a reasonable distance higher or lower (in IM-terms) than the base case median.

In view of the above, Figure 5(a) is clear-cut: Increasing or decreasing the yield strength of the plastic hinges through a_{My} does indeed cause an almost equal increase or decrease, respectively, of the seismic capacity of most post-yield limit-states. Actually this is the only parameter whose variability is propagated practically unchanged through the model; the other five parameters generally show much reduced effectiveness. Figure 5(b) shows one such case where both a large increase and a decrease of the hardening slope a_h seem to offer only a 10% respective change in global collapse capacity. On the other hand, accelerating or delaying the occurrence of the strength drop is of decisive importance (Figure 5(c)). Increasing μ_c to 4 has produced an almost 20% improvement practically everywhere in the median capacities after 3% interstory drift. Reducing μ_c to 2 has a -20% impact on the structural capacity as the accumulation of serious damage begins much earlier in the point hinges. The impact of a_c is shown in Figure 5(d) where, as expected, reducing (in absolute terms) the negative slope provides benefits up to 10% while making it steeper has a 15-20% detrimental effect. As discussed previously, the relatively low value of these sensitivities is a direct result of the relatively high default residual plateau; at $r = 50\%$ it tends to trim down the effect of the negative drop, thus reducing its importance.

Figure 5(e) shows the effect of r, where it appears that for a given negative drop and a relatively short plateau ($\mu_u = 6$), the residual moment of the plastic hinge has little influence on the predicted performance of the LA9 structure. However, different default settings on a_c and μ_u can easily change such results; therefore no general conclusions should be drawn just yet. On the other hand, for μ_u there can be no objection that the median IDAs are greatly influenced by its reduction but not significantly by its increase (Figure 5(f)). A 33% decrease in ultimate-ductility cost the structure a 40% reduction in collapse capacity, while an equal

improvement made no difference statistically. It seems that the strength loss caused by a brittle and fracturing connection will dominate the response of the building. On the other hand, even a substantial increase in the rotational ductility does not make much difference for this building, perhaps because of other mechanisms or effects, e.g., P-Δ, taking the lead to cause collapse. In other words, even letting μ_u go to infinity, as is typically assumed by most existing models, we would not see much improvement as the building has already benefited from ultimate rotational ductility as much as it could.

5. UNCERTAINTY ANALYSIS

In order to evaluate the effect of uncertainties on the seismic performance of the structure we chose to vary the base-case beam-hinge backbone by assigning probabilistic distributions to its six parameters. Since existing literature does not provide adequate guidance on the properties of all six variables, we chose to arbitrarily define them. Thus, each parameter is assumed to be independently normally distributed with a mean equal to its default value and a coefficient of variation (c.o.v) equal to 0.2 for a_{My} (due to its overwhelming effect) and 0.4 for the remaining five parameters. Since the normal distribution assigns non-zero probabilities even for physically impossible values of the parameters, e.g., $r < 0$, or $a_h > 1$ we have truncated the distribution of each parameter within a reasonable minimum and maximum that satisfies the physical limits. We chose to do so by setting hard limits at 1.5 standard deviations away from the central value, thus cutting off only the most extreme cases as shown in Table II. All distributions where appropriately rescaled to avoid the concentration of high probabilities at the cutoff points [20].

Table II. The distribution properties of the uncertain parameters.

	mean	c.o.v	min	max	type
a_{My}	1.0	20%	0.70	1.30	truncated normal
a_h	0.1	40%	0.04	0.16	truncated normal
μ_c	3.0	40%	1.20	4.80	truncated normal
a_c	-0.5	40%	-0.80	-0.20	truncated normal
r	0.5	40%	0.20	0.80	truncated normal
μ_u	6.0	40%	2.40	9.60	truncated normal

5.1. Monte Carlo with LHS

Faced with the non-existence of a closed-form solution for the seismic response of a complex nonlinear model, there are few routes we can follow to estimate its variability. The most comprehensive, but at the same time most computationally expensive, solution is the Monte Carlo simulation. By sampling N times from the parameter distributions, Monte Carlo creates a population of N possible instances of the structure, each of which needs to be analyzed. Assuming a large enough number of structures has been sampled, we can reliably estimate the full distribution of the seismic performance of the structure.

Monte Carlo simulation can be further improved by replacing the classic random sampling of the population with latin hypercube sampling (LHS, McKay *et al.* [21]). Similar conclusions

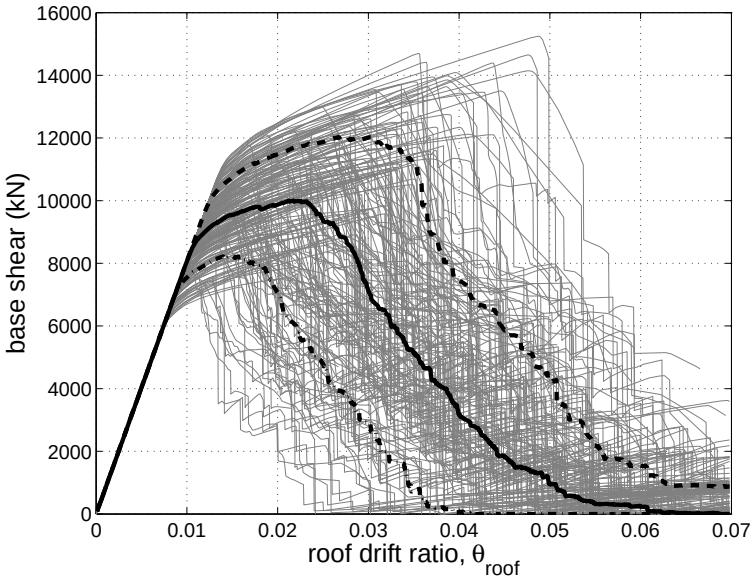

Figure 6. 200 static pushover curves shown against the 16, 50, 84% fractile curves of base shear given θ_{roof}.

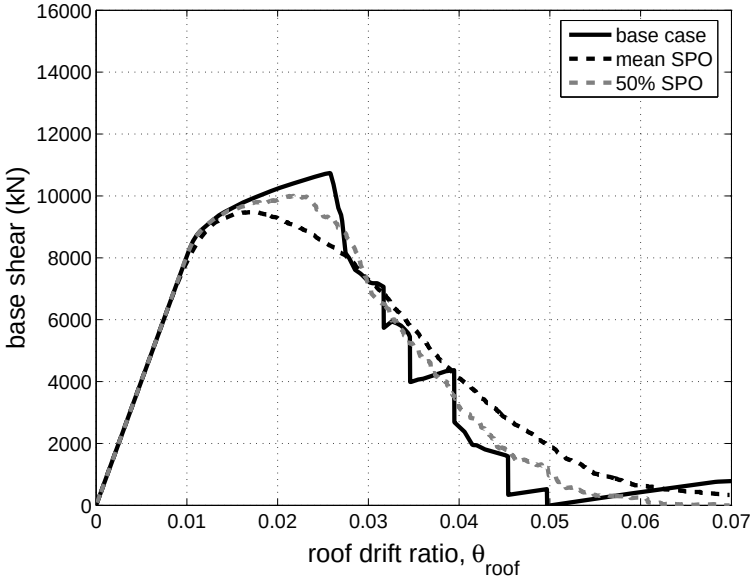

Figure 7. The mean and median pushover curves compared against the base case.

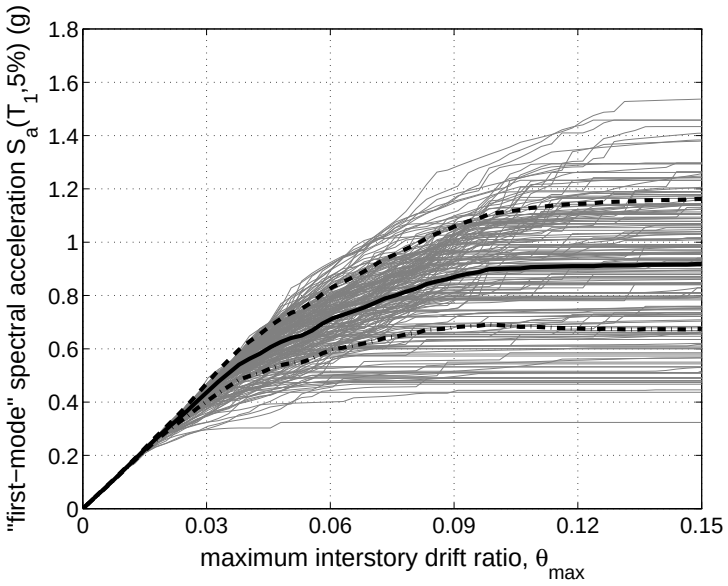

Figure 8. 200 median IDAs shown against their mean and ± one standard deviation curves of $S_a(T_1, 5\%)$ given $\theta_{\max}$. The corresponding 16, 50 and 84% fractiles are practically coincident with the mean-sigma, mean and mean+sigma curves shown.

have been reached earlier by Dolsek [11] who has also chosen this route to handle the parameter uncertainties within IDA. This makes absolute sense as LHS is a special case of stratified sampling that allows efficient estimation of the quantity of interest by reducing the variance of classic Monte Carlo. While random sampling produces standard errors that decline with $\sqrt{N}$, the error in LHS goes down much faster, approaching the rate of $\sqrt{N^3}$ for linear functions (Iman [22]). In other words, we can reduce the number of simulations needed to achieve the desired confidence in our results by a factor of N^2 at best. This might seem trivial, especially since most people might think of buildings as highly nonlinear creatures. Actually, buildings are only mildly nonlinear in functional terms, especially compared to physical processes (e.g., weather forecasting), since most nonlinearity is isolated in relatively few elements of the model. This is actually one of the reasons why simple elastic analysis or modal combination rules still remain useful in structural analysis. Thus LHS is ideally suited to reducing the dispersion of Monte Carlo simulation on nonlinear structures.

Unfortunately, the nature of LHS does not allow us to determine *a priori* the appropriate sample size N to achieve a certain confidence level (Iman [22]). Still, the use of a relatively high N that is at substantially larger than the number of parameters will always result to reasonably accurate estimates for practical purposes. The optimal N to use is obviously a function of the number of random variables and their influence on the response; this remains a subject of further research. In our case, Monte Carlo with latin hypercube sampling was performed for $N = 200$ realizations of the frame, a relatively high number (compared to e.g., Dolsek [11]) that was chosen to allow pinpoint accuracy in our estimates. To further improve the quality of our calculations, we employed the Iman and Conover [23] algorithm to reduce

any spurious correlation appearing between the samples.

To provide some insight on the range of models generated, their SPO curves were evaluated and plotted in Figure 6. Therein, the flexibility of our model becomes apparent: The sample ranges from ultra-ductile systems that continue to gain strength up to 4.5% roof drift down to brittle frames that rapidly lose strength after only 1.5% roof drift. The maximum and minimum strengths are equally impressive, varying within 7000–15000kN. The 16, 50, 84% fractile pushover curves of base shear given θ_{roof} also appear in Figure 6, showing a coefficient of variation that rapidly increases with θ_{roof}: Starting from zero, in the elastic range, it goes almost to 100% at θ_{roof} =4%, being dominated by the decreasing value of base shear and the relatively constant standard deviation. Clearly, the wide distribution of the beam-hinge parameters has produced a very diverse sample of structures.

As an early taste of discussions to follow, Figure 7 shows a comparison of the mean pushover curve versus the base case pushover, i.e., a comparison of the actual mean response versus the response of the mean model. Considering the excellent accuracy offered by the $N = 200$ samples, there is obviously a clear violation of the typical first-order assumption: the mean response is not the same as the response of the mean structure. On the other hand, the median pushover curve is quite closer to the base case, although some differences are still there. Nevertheless, for engineering purposes, one can still argue that the differences shown might not be significant. It remains to be seen whether such observations in the pushover space actually translate to similar conclusions in the IDA results.

Thus, by performing IDA on each of the N samples we have obtained $30 \times N = 6000$ IDA curves and the $N = 200$ corresponding median IDAs shown in Figure 8. The variability in the results is apparent, even within just the medians: Showing a similar spread to the pushover results (Figure 6), there exist realizations of the nine-story structure that collapse for half the records at $S_a(T_1, 5\%)$-values as low as 0.3g, while others remain stable up to 1.5g, the average case having a (median) capacity of about 0.9g. In order to draw useful conclusions from such results, we need to quantify and simplify the probabilistic nature of the curves. Therefore, we have to estimate their moments. We will attempt to do so first by taking advantage of the Monte Carlo results (Figure 8) and then by attempting simpler approximations that bypass the cumbersome Monte Carlo simulation.

5.2. Moment Estimation via Monte Carlo

In our development we are interested in estimating a central value and a dispersion for the S_a-values of capacity for a given limit-state defined at a specific value of $\theta_{\max}$. As a central value we will use the median of the $S_a(T_1, 5\%)$-capacities given $\theta_{\max}$, $\Delta_{S_a|\theta_{\max}}$, while the dispersion caused by the uncertainty in the median capacity will be characterized by its β-value, [24], i.e., the standard deviation of the natural logarithm of the median S_a-capacities conditioned on $\theta_{\max}$: $\beta_U = \sigma_{\ln S_a|\theta_{\max}}$. In terms of the work of Jalayer [25] we will be essentially adopting the IM-based method of estimating the mean annual frequency of limit-state exceedance. Since we will be implicitly using all S_a-related quantities as conditioned on $\theta_{\max}$, we will simplify notation by dropping the conditioning "$\ldots|\theta_{\max}$" from all formulas.

Thus, let $\ln S_a^{i,j}$ be the natural log of the S_a-capacity for a given value of $\theta_{\max}$, structure j ($j = 1, \ldots, N$) and record i ($i = 1, \ldots, P$), while $\overline{\ln S_a}$ is the overall mean of the log-capacities. Then, $\ln S_{a,50\%}^{j}$ is the log of their median value for a structure j, and $\overline{\ln S_{a,50\%}}$ is the mean of the corresponding natural logarithms of the medians over all samples. We can obtain the

overall median Δ_{S_a}, its dispersion β_U due to parameter uncertainty and the total dispersion β_{RU} due to both uncertainty and record-to-record variability as:

$$\Delta_{S_a} = \text{med}_j \left(S^j_{a,50\%} \right) \approx \overline{\ln S_{a,50\%}} \approx \overline{\ln S_a} \tag{1}$$

$$\beta_U = \sqrt{\frac{\sum_{j=1}^{N} \left(\ln S^j_{a,50\%} - \overline{\ln S_{a,50\%}} \right)^2}{N-1}} \tag{2}$$

$$\beta_{RU} = \sqrt{\frac{\sum_{j=1}^{N} \sum_{i=1}^{P} \left(\ln S^{i,j}_a - \overline{\ln S_a} \right)^2}{NP-1}} \tag{3}$$

where "med_j" is the median operator over all indices (structures) j. It is worthwhile to note that since all sampled structures were analyzed with the same number of records ($P = 30$), if we took the mean-log of all $NP = 6000$ single-record IDA curves, we would find the same results as with taking the mean of the $N = 200$ mean-log (or median) capacities. This is where the last approximate equality in Equation 1 comes from.

5.3. Point estimate methods

Point estimate methods (PEM) can be used to calculate the first few moments of a function in terms of the first moments of the random variables. Rosenblueth's $2K+1$ method [26] is based on a finite difference concept and is one of the easiest point estimate methods to implement. In essence, it is a simulation technique that requires $2K+1$ simulations, where K is the number of random variables. The advantage of the method is that it does not require knowledge of the distribution of the random variables since only the first two moments are sufficient. To apply it for our purpose, the log of the median S_a-capacities given $\theta_{\max}$ is considered a function of the six random parameters,

$$\ln S_{a,50\%} = f(\mathbf{X}) = f(a_{\text{My}}, a_h, \mu_c, a_c, r, \mu_u) \tag{4}$$

where f is a function (with unknown analytical form) of the random variables for the given limit-state (i.e., value of $\theta_{\max}$ considered) and $\mathbf{X} = [a_{\text{My}}, a_h, \mu_c, a_c, r, \mu_u]$ is the vector of the random modeling parameters.

First of all, PEM requires the evaluation of $\ln S^0_{a,50\%}$, the base-case value of f that corresponds to all random variables being set equal to their mean m_{X_k}. The remaining $2K$ simulations are obtained by shifting each parameter X_k ($k = 1, \ldots, 6$) from its mean by $\pm\sigma_{X_k}$ while all other variables remain equal to their mean m_{X_k}. When the X_k parameter is perturbed, the logs of the median S_a-capacities are denoted as $\ln S^{k+}_a$ and $\ln S^{k-}_a$, where the sign indicates the direction of the shift. For example, if the 4th parameter, $X_4 = a_c$, is perturbed, then the corresponding capacities are calculated as:

$$\ln S^{4\pm}_a = f\left(m_{a_{\text{My}}}, m_{a_h}, m_{\mu_c}, m_{a_c} \pm \sigma_{a_c}, m_r, m_{\mu_u}\right) \tag{5}$$

Based on Equation 5, the conditional mean and coefficient of variation (c.o.v) of S_a are:

$$m_{\ln S_a} = \ln S^0_{a,50\%} \prod_{k=1}^{K} \frac{\ln S_a^{k+} + \ln S_a^{k-}}{2 \ln S^0_{a,50\%}} \tag{6}$$

$$V_{\ln S_a} = \sqrt{\left\{ \prod_{k=1}^{K} \left[1 + \left(\frac{\ln S_a^{k+} - \ln S_a^{k-}}{\ln S_a^{k+} + \ln S_a^{k-}} \right)^2 \right] \right\} - 1} \tag{7}$$

Then, assuming lognormality, the median $S_a|\theta_{\max}$ and the dispersion β_U can be estimated as:

$$\Delta_{S_a} = \exp\left(m_{\ln S_a}\right) \tag{8}$$

$$\beta_U = m_{\ln S_a} \cdot V_{\ln S_a} \tag{9}$$

For every limit-state, Equations 5–9 are used to estimate the median IDA curve and the β-dispersion values with only $2K + 1$ IDA simulations.

5.4. First-Order Second-Moment method

The first-order second moment (FOSM) method is another easy-to-implement approximating method that can be used to calculate the first moments of a nonlinear function, and has often been used to estimate uncertainty (e.g., Lee and Mosalam [7], Baker and Cornell [27]) The number of simulations required is only $2K + 1$, equal to that of the PEM, while it also does not require prior knowledge of the distribution of the random parameters. According to FOSM, the unknown, in closed form, nonlinear function f can be approximated through the use of a Taylor expansion to obtain its first and second moments. Following the notation of Equation 4, the function $f = \ln S_a$ is approximated using Taylor series expansion around the mean $\overline{\mathbf{X}} = \left[m_{a_{\mathrm{My}}}, m_{a_h}, m_{\mu_c}, m_{a_c}, m_r, m_{\mu_u}\right]$. Assuming that the random variables are not correlated, the approximation takes the form (Pinto *et al.* [28]):

$$f(\mathbf{X}) \approx f\left(\overline{\mathbf{X}}\right) + \sum_{k=1}^{K} \left(X_k - m_{X_k}\right) \left.\frac{\partial f}{\partial X_k}\right|_{\overline{\mathbf{X}}} + \frac{1}{2} \sum_{k=1}^{K} \left(X_k - m_{X_k}\right)^2 \left.\frac{\partial^2 f}{\partial X_k^2}\right|_{\overline{\mathbf{X}}} \tag{10}$$

The gradient and curvature of f can be approximated with a finite difference approach, which is why we need $2K+1$ simulations. The random parameters are set equal to their mean to obtain S_a^0 and then each random parameter is perturbed according to Equation 5. Thus, the first and the second derivative of f with respect to X_k, will be:

$$\frac{\partial f}{\partial X_k} \approx \frac{\ln S_a^{k+} - \ln S_a^{k-}}{2\sigma_{X_k}} \tag{11}$$

$$\frac{\partial^2 f}{\partial X_k^2} \approx \frac{\ln S_a^{k+} - 2 \ln S_a^0 + \ln S_a^{k-}}{\sigma_{X_k^2}} \tag{12}$$

Truncating after the linear terms in Equation 10 provides a first-order approximation for the limit-state mean-log capacities, where essentially they are assumed to be equal to the base-case values $\ln S_a^0$. A more refined estimate is the mean-centered, second-order approximation, which according to Equation 10 can be estimated as:

$$m_{\ln S_a} \approx \ln S^0_{a,50\%} + \frac{1}{2} \sum_{k=1}^{K} \left.\frac{\partial^2 f}{\partial X_k^2}\right|_{\overline{\mathbf{X}}} \sigma_{X_k^2} \tag{13}$$

Thus the median S_a capacity, assuming lognormality, comes out to be:

$$\Delta_{S_a} = \exp\left(m_{\ln S_a}\right) \tag{14}$$

while, using a first-order approximation, the standard deviation of the logs is estimated as:

$$\beta_U \approx \sum_{k=1}^{K} \left(\frac{\partial f}{\partial X_k}\bigg|_{\overline{\mathbf{X}}} \right)^2 \sigma_{X_k}^2. \tag{15}$$

5.5. Median and Dispersion Estimates

The results of all three methods for the overall median IDA curve appear in Figure 9(a). FOSM and PEM offer almost identical estimates of the median, which are very accurate up to $\theta_{\max} = 5\%$ but tend to oscillate off the mark and underpredict the LHS results for all higher limit-states. Interestingly enough, the LHS median of all sample medians shows a collapse capacity of 0.9g, i.e., 0.1g lower than the base case median of almost 1.0g. Given the dispersion shown and the sample size used, this difference becomes *statistically* significant at the 95% confidence level. Thus, considerable doubt is cast on the typical, first-order assumption that the median-parameter model will produce the median seismic performance (e.g., [24]). Still, the 10% error found in this case may only be of theoretical interest; it should not be considered important for practical applications. Were this difference any larger, it could have far-reaching implications: Almost all building analyses executed by engineers utilize central values (means or medians) for the parameters, implicitly aiming to estimate the "central value" (mean or median) of response. This is only *approximately* true for the structure studied.

In order to better understand the reasons behind this apparent disagreement with current engineering intuition, we have repeated the simulation for a deterministic $\mu_u = 6$ and only five random parameters using $N = 120$ samples. The resulting medians, appearing in Figure 9(b), show a much improved picture that is now closer to what we might normally expect. While there is still a statistically-significant difference (at 95% confidence) of about 4% between the base-case and the LHS median, the two curves are practically indistinguishable from each other. Even the PEM and FOSM approximations perform much better and manage to provide a good estimate. Thinking back to the extremely asymmetric influence of μ_u on the median IDAs (Figure 5(f)) it becomes apparent that the unbalanced response of the system to changes in μ_u is the reason why the overall median has been dragged down and away from the response of the median-parameter model. Still, this is not an isolated case by any means. Structures under earthquake loads can be visualized as links in a chain: A series system of collapse mechanisms. The weakest link will always cause collapse. As long as we keep sampling from the distributions of the parameters, the capacity of some mechanisms will be increased and for others it will decrease. Similar conclusions have been drawn for a reinforced concrete frame by Liel *et al.* [10]. Thus, on average, we should always expect that the overall median/mean capacity will be lower than the capacity of the median/mean model, even if by a little. The number of asymmetric sensitivity plots in Figure 5 should provide ample warning.

As a postscript to the discussion of medians, it should be noted that the approximate FOSM and PEM-derived median $S_a(T_1, 5\%)$-given-$\theta_{\max}$ results in Figures 9(a)–(b) cannot be thought of as IDA curves in the classical form; the reason is that due to the inverse method of their construction, there are multiple values of $\theta_{\max}$-demand for a given value of $S_a(T_1, 5\%)$. To rectify this issue, one can simply apply a monotone smoother (e.g., Zhang [29]) and obtain

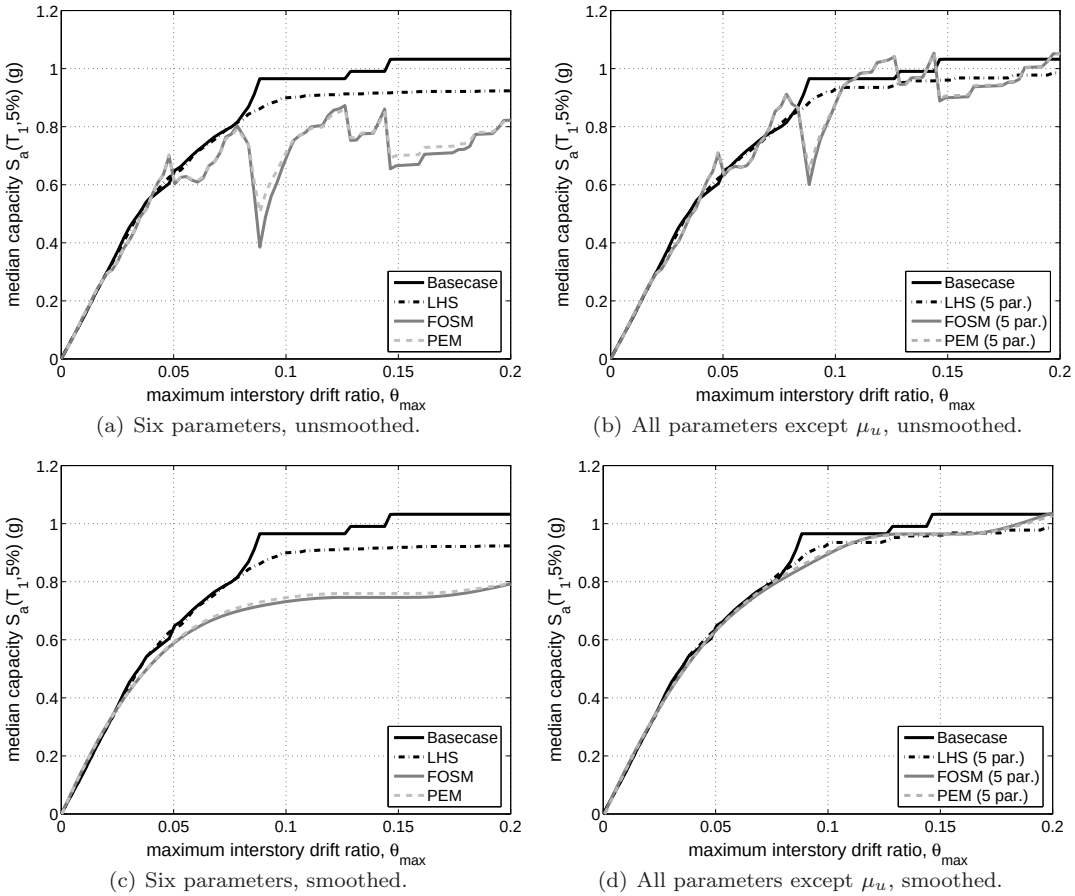

(a) Six parameters, unsmoothed.
(b) All parameters except μ_u, unsmoothed.
(c) Six parameters, smoothed.
(d) All parameters except μ_u, smoothed.

Figure 9. Median IDA curves estimated for 6 or 5 parameters using LHS, FOSM and PEM.

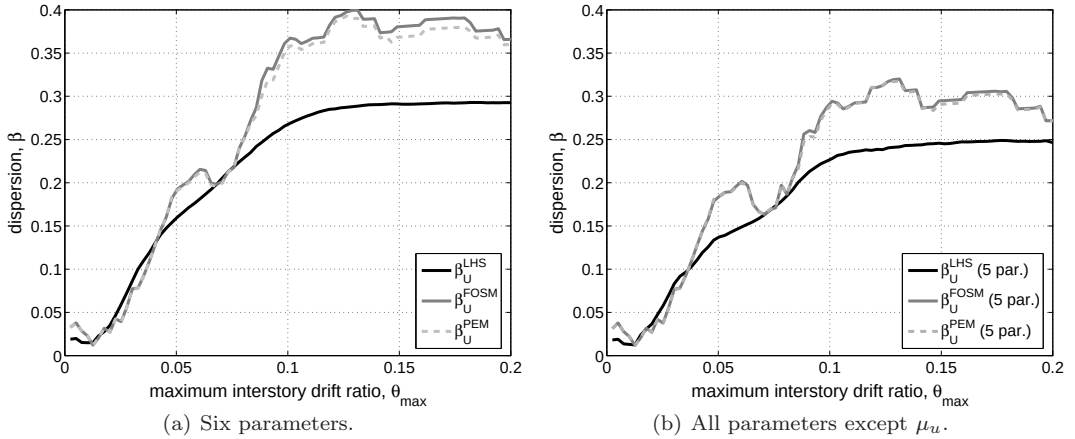

(a) Six parameters.
(b) All parameters except μ_u.

Figure 10. Values of β_U given $\theta_{\max}$ estimated for 6 or 5 parameters using LHS, FOSM and PEM.

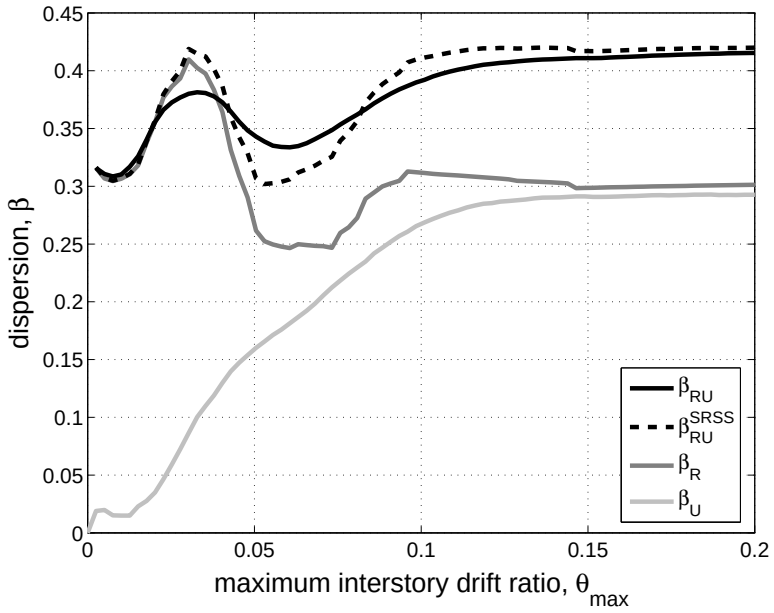

Figure 11. The values of β_U, β_R, β_{RU} compared against the SAC/FEMA approximation β_{RU}^{SRSS} given $\theta_{\max}$.

the perfectly acceptable curves shown in Figures 9(c)–(d). Such methods, though, need IDA-quality data to work with. When performing a limited performance estimation using dynamic runs at a single IM-level, it would be advisable to stay with the base case or, even better, use Monte Carlo with LHS for a reasonable estimate of the median.

The estimates of β_U obtained by the three methods for six and five random parameters appear in Figures 10(a) and 10(b), respectively. In all cases the epistemic uncertainty smoothly rises from a zero value in the elastic range (reasonable, as all modifications to the plastic hinges are post-yield) and slowly increases up to its collapse-level value. For the six-parameter case this is estimated to be $\beta_U = 0.30$ by Monte Carlo, while both PEM and FOSM manage to get quite close, moderately overpredicting the dispersion at collapse as 0.36, showing errors of 20–25%. Obviously, both methods can provide a usable estimate to β_U using only $2\times6+1 = 13$ sample points, rather than 120–200 for LHS. That is almost an order-of-magnitude reduction in computations at the cost of a reasonable error. Monte Carlo might become more competitive at lower sample sizes [11], but as discussed, coming up with an appropriate number *a priori* can be difficult. A different strategy aimed at reducing the computational load can be found in Fragiadakis and Vamvatsikos [30], using static pushover analyses rather than IDA.

In terms of combining epistemic uncertainty and aleatory randomness, the epistemic uncertainty β_U is competing against the dispersion due to record-to-record variability of $S_a(T_1, 5\%)$ given the EDP $\theta_{\max}$. This dispersion is also important for the performance evaluation of structures and similarly represented by its β-value [1], i.e., by the standard deviation of the natural logarithm of the IM given the EDP. This can be directly estimated from the sample IDA curves of the base case, as we will do, or it can be approximated from

the corresponding fractile IDAs as

$$\beta_R \approx \frac{1}{2}\left(\ln S_a^{84\%} - ln S_a^{16\%}\right), \tag{16}$$

where $S_a^{84\%}$ and $S_a^{16\%}$ are the 84% and 16% values of $S_a(T_1, 5\%)$-capacity.

Both the epistemic uncertainty β_U and the aleatory randomness β_R contribute to the value of the total dispersion β_{RU} caused by the record-to-record randomness and the model uncertainty. This is often used, e.g., in the SAC/FEMA framework, to assess performance in the presence of uncertainty (Cornell *et al.* [24]). Since we have available the full IDA data from the Monte Carlo simulation, we can estimate β_{RU} directly from the 200×30 single-record IDA curves (Equation 3). Alternatively, SAC/FEMA [1] estimates β_{RU} as the square-root-sum-of-squares (SRSS) of β_R and β_U, an approximation which is usually taken for granted:

$$\beta_{RU}^{SRSS} = \sqrt{\beta_R^2 + \beta_U^2} \tag{17}$$

Such a value for every limit-state, or value of $\theta_{\max}$, serves as a useful comparison of the relative contribution of randomness and uncertainty to the total dispersion as shown in Figure 11. Of course, we should keep in mind that we are only showing a simple example that does not include all possible sources of uncertainty. Therefore, any conclusions that we draw should be viewed in light of these limitations.

Having said that, in our case the high β_R generally overshadows the lower β_U, despite the use of perfect spatial correlation and moderate-to-high values for the parameter c.o.v of 0.2 to 0.4. The record-to-record variability is higher for any limit-state, ranging from 0.30 up to 0.40. Still, the β_U increases rapidly as the structure approaches global dynamic instability. At such higher limit-states the uncertainty caused by all parameters rises to such an extent that β_U can almost reach, in this example, the corresponding value of β_R; 0.29 for β_U versus 0.31 for β_R. Finally we see that the SRSS estimate of β_{RU} is very close to its value estimated by LHS. On average Equation (17) accurately predicts the actual β_{RU}. The error is in the order of 5% or less, except for drifts within 0.05 to 0.08 where the error grows to almost 20%. For all practical purposes, the SRSS rule for combining aleatory randomness and epistemic uncertainty can be considered accurate for this structure.

As a final comment we have produced histograms showing the probabilistic distributions of $S_a(T_1, 5\%)$-values of capacity for four limit-states, i.e., conditional on $\theta_{\max} = 0.03$, 0.06, 0.09, 0.12. Figure 12 presents the distribution of the median $S_a(T_1, 5\%)$ due to parameter epistemic uncertainty and Figure 13 shows the distribution of $S_a(T_1, 5\%)$ due to combined epistemic and aleatory variability. In other words, β_U and β_{RU} can be estimated for each of the four $\theta_{\max}$-values by calculating the standard deviation of the natural logs of the $S_a(T_1, 5\%)$-data contained in Figures 12 and 13 respectively.

To better judge the distribution of this data we have also plotted the best-fit normal density function. Obviously the actual distributions are only approximately symmetric and slightly skewed to the right. Having used normal distributions for the parameters, the epistemic uncertainty in $S_a(T_1, 5\%)$ also comes out to be approximately normal. Kolmogorov-Smirnov distribution tests [20] confirm the appropriateness of the normality assumption at the 95% level for all but the lowest values of $\theta_{\max}$. On the other hand, the lognormality assumption is rejected. Furthermore, the heavy tail of the record-to-record variability skews the combined aleatory plus epistemic uncertainty to the right, pushing it closer to the lognormal rather than

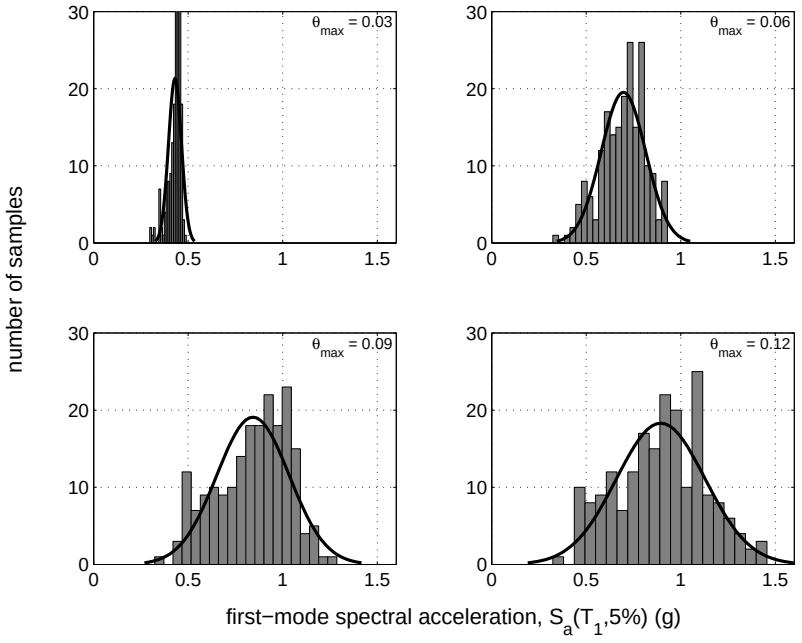

Figure 12. The distribution due to epistemic uncertainty of the median $S_a(T_1, 5\%)$-values of capacity, given four values of $\theta_{\max}$.

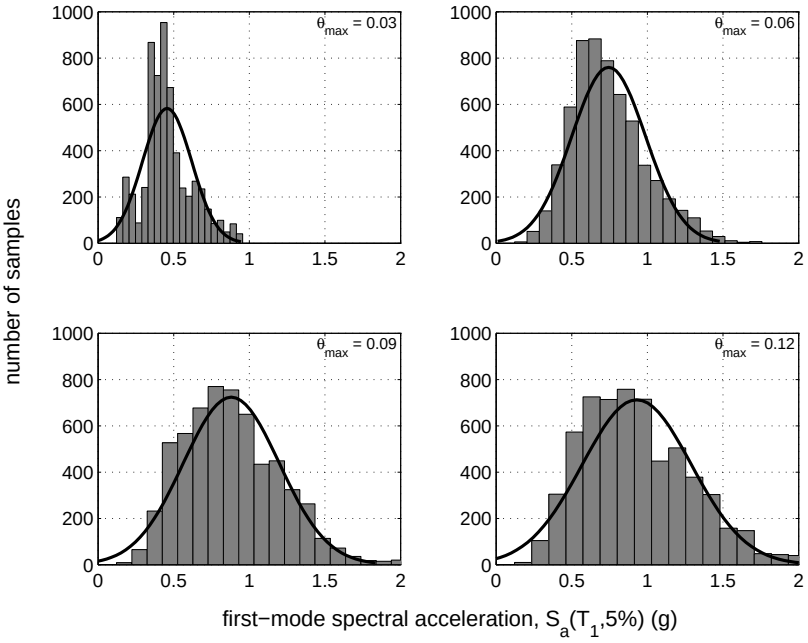

Figure 13. The distribution due to both epistemic and aleatory uncertainty of the $S_a(T_1, 5\%)$-values of capacity given four values $\theta_{\max}$.

the normal. This trend becomes more prominent for the lower values of $\theta_{\max}$ where β_R is dominant (Figure 11). Still, statistical tests at the 95%, or even the 90% level do not confirm the feasibility of either of the two distributions. In other words, the theoretically-attractive lognormal assumption may be good enough for the record-to-record variability, but, depending on the assumed distribution of model parameters, it may not be appropriate for the epistemic uncertainty or the combined total.

6. CONCLUSIONS

The parameter sensitivity and epistemic uncertainty in the seismic demand and capacity of a nine-story steel moment-resisting frame with non-deterministic beam-hinges have been estimated using IDA. Sensitivity results have shown the differing effect of the hinge moment-rotation backbones to the system's behavior: While the yield moment, the capping ductility, the negative stiffness ratio and the ultimate ductility have a significant impact, the hardening stiffness ratio and the residual moment are only marginally important. In addition, in line with recent research, Monte Carlo simulation with latin hypercube sampling has been employed as the primary means to propagate the uncertainty from the model parameters to the seismic performance, while simplified methods based on point-estimate methods and first-order second-moment techniques have also been proven to allow accurate estimation at a fraction of the cost of simulation.

All in all, the epistemic uncertainty in beam-hinges is shown to be an important contributor to the overall dispersion in the performance estimation as well as a key point that raises issues regarding the validity of current assumptions in performance evaluation. The classic notion that the median-parameter model produces the median seismic demand and capacity has been disproved. Nevertheless, the error is low enough that it can still be considered as reasonably accurate for practical applications. Finally, the simple square-root-sum-of-squares rule for the combination of aleatory randomness with epistemic uncertainty has been proven to be accurate enough for some limit-states but significantly off the mark for others. In summary, corroborating existing research, IDA has been shown to possess the potential to become the standard for performance uncertainty estimation. Although resource-intensive and sometimes controversial for using record-scaling, it can be used as a basis for developing and validating simpler methodologies that can provide reliable results at a reduced computational cost.

ACKNOWLEDGEMENT

The first author wishes to gratefully acknowledge the everlasting friendship and support of Professor C. Allin Cornell who was lost to us on December 14th, 2007.

REFERENCES

1. SAC/FEMA. Recommended seismic design criteria for new steel moment-frame buildings. *Report No. FEMA-350*, SAC Joint Venture, Federal Emergency Management Agency, Washington, DC, 2000.
2. Luco N, Cornell CA. Effects of random connection fractures on demands and reliability for a 3-story pre-Northridge SMRF structure. In *Proceedings of the 6th U.S. National Conference on Earthquake Engineering*, Paper No. 244. EERI, El Cerrito, CA: Seattle, WA, 1998; 1–12.

3. Luco N, Cornell CA. Effects of connection fractures on SMRF seismic drift demands. *ASCE Journal of Structural Engineering* 2000; **126**:127–136.
4. Foutch DA, Shi S. Effects of hysteresis type on the seismic response of buildings. In *Proceedings of the 6th U.S. National Conference on Earthquake Engineering*, Paper No. 409. EERI, El Cerrito, CA: Seattle, WA, 1998; 1–12.
5. Ibarra LF. Global collapse of frame structures under seismic excitations. PhD Dissertation, Department of Civil and Environmental Engineering, Stanford University, Stanford, CA, 2003.
6. Porter KA, JL JLB, Shaikhutdinov RV. Sensitivity of building loss estimates to major uncertain variables. *Earthquake Spectra* 2002; **18**(4):719743.
7. Lee TH, Mosalam KM. Seismic demand sensitivity of reinforced concrete shear-wall building using FOSM method. *Earthquake Engineering and Structural Dynamics* 2005; **34**(14):17191736.
8. Rubinstein RY. *Simulation and the Monte Carlo method*. John Wiley & Sons: New York, 1981.
9. Vamvatsikos D, Cornell CA. Incremental dynamic analysis. *Earthquake Engineering and Structural Dynamics* 2002; **31**(3):491–514.
10. Liel AB, Haselton CB, Deierlein GG, Baker JW. Incorporating modeling uncertainties in the assessment of seismic collapse risk of buildings. *Structural Safety* 2009; **31**(2):197–211.
11. Dolsek M. Incremental dynamic analysis with consideration of modelling uncertainties. *Earthquake Engineering and Structural Dynamics* 2009; **38**(6):805–825.
12. Foutch DA, Yun SY. Modeling of steel moment frames for seismic loads. *Journal of Constructional Steel Research* 2002; **58**:529–564.
13. McKenna F, Fenves G, Jeremic B, Scott M. Open system for earthquake engineering simulation, 2000. URL http://opensees.berkeley.edu. [May 2008].
14. Fragiadakis M, Vamvatsikos D, Papadrakakis M. Evaluation of the influence of vertical irregularities on the seismic performance of a 9-storey steel frame. *Earthquake Engineering and Structural Dynamics* 2006; **35**(12):1489–1509.
15. Vamvatsikos D, Cornell CA. Developing effcient scalar and vector intensity measures for IDA capacity estimation by incorporating elastic spectral shape information. *Earthquake Engineering and Structural Dynamics* 2005; **34**(13):1573–1600.
16. Luco N, Bazzurro P. Does amplitude scaling of ground motion records result in biased nonlinear structural drift responses? *Earthquake Engineering and Structural Dynamics* 2007; **36**(13):1813–1835.
17. Luco N, Cornell CA. Structure-specific, scalar intensity measures for near-source and ordinary earthquake ground motions. *Earthquake Spectra* 2007; **23**(3):357–392.
18. Baker JW, Cornell CA. Vector-valued intensity measures incorporating spectral shape for prediction of structural response. *Journal of Earthquake Engineering* 2008; **12**(4):534–554.
19. Vamvatsikos D, Cornell CA. Applied incremental dynamic analysis. *Earthquake Spectra* 2004; **20**(2):523–553.
20. Benjamin JR, Cornell CA. *Probability, Statistics, and Decision for Civil Engineers*. McGraw-Hill: New York, 1970.
21. McKay MD, Conover WJ, Beckman R. A comparison of three methods for selecting values of input variables in the analysis of output from a computer code. *Technometrics* 1979; **21**(2):239–245.
22. Iman R. *Latin Hypercube Sampling*. In: Encyclopedia of Statistical Sciences. Wiley: New York. DOI: 10.1002/0471667196.ess1084.pub2.
23. Iman RL, Conover WJ. A distribution-free approach to inducing rank correlation among input variables. *Communication in Statistics Part B: Simulation and Computation* 1982; **11**(3):311–334.
24. Cornell CA, Jalayer F, Hamburger RO, Foutch DA. The probabilistic basis for the 2000 SAC/FEMA steel moment frame guidelines. *ASCE Journal of Structural Engineering* 2002; **128**(4):526–533.
25. Jalayer F. Direct probabilistic seismic analysis: Implementing non-linear dynamic assessments. PhD Dissertation, Department of Civil and Environmental Engineering, Stanford University, Stanford, CA, 2003. URL http://www.stanford.edu/group/rms/Thesis/FatemehJalayer.pdf. [Oct 2008].
26. Rosenblueth E. Point estimates for probability. *Applied Mathematical Modeling* 1981; **5**:329–335.
27. Baker JW, Cornell CA. Uncertainty propagation in probabilistic seismic loss estimation. *Structural Safety* 2008; **30**(3):236–252.
28. Pinto PE, Giannini R, Franchin P. *Seismic Reliability Analysis of Structures*. IUSS Press: Pavia, Italy, 2004.
29. Zhang JT. A simple and efficient monotone smoother using smoothing splines. *Journal of Nonparametric Statistics* 2004; **16**(5):779–796.
30. Fragiadakis M, Vamvatsikos D. Fast performance uncertainty estimation via pushover and approximate IDA. *Earthquake Engineering and Structural Dynamics* 2009; (in review).